Carbon Monoxide Adsorption and Oxidation on Monolayer Films of Cubic Platinum Nanoparticles Investigated by Infrared−Visible Sum Frequency Generation Vibrational Spectroscopy

S. J. Kweskin,[†,‡] R. M. Rioux,[†,§] S. E. Habas,[†] K. Komvopoulos,[‡] P. Yang,[†] and G. A. Somorjai*[,†]

Department of Chemistry, University of California, Berkeley, California 94720, and Materials Sciences Division, Lawrence Berkeley National Laboratory, Berkeley, California 94720, and Department of Mechanical Engineering, University of California, Berkeley, California 94720

Received: April 19, 2006; In Final Form: June 14, 2006

The adsorption and oxidation of CO on monolayer films of cubic Pt nanoparticles synthesized by a modified solution-phase polyol process were examined by sum frequency generation (SFG) vibrational spectroscopy in total internal reflection (TIR) geometry. Extremely low incident laser power (∼5 μJ/pulse of infrared) yields sufficient SFG intensity in TIR geometry and reduces destructive interference. Because TIR-SFG spectroscopy does not require correction for bulk gas absorption, CO spectra can be collected over a wide pressure range (<1 mTorr up to 700 Torr). Poly(vinylpyrrolidone)-capped Pt nanoparticles deposited on single-crystal sapphire were monitored under high-pressure reaction conditions in a combined spectroscopy-catalytic reactor cell. The effect of the capping polymer on the position and intensity of the CO peak was studied before and after low-temperature calcination. The polymer decreased the amount of CO adsorption and caused a slight red-shift of the atop CO band relative to a surface treated in oxygen at 373 K. Oxidation rates were determined by measuring the intensity of the atop CO peak as a function of time in the presence of flowing oxygen. The activation energy (∼19.8 kcal/mol) determined from the SFG data is close to that obtained from gas chromatography (GC) measurements of CO oxidation rates at different temperatures. The SFG and GC results are in good agreement with published data for Pt(100) surfaces.

1. Introduction

Studies on single crystals and nanoparticles have demonstrated differences in the reactivity of terrace atoms and less coordinated surface atoms, such as those at steps and kinks.[1−3] Adsorption and reactions at corner and edge atoms, which are prevalent in nanoparticles but mostly absent from high-coordination single-crystal surfaces, such as Pt(100) and Pt-(111), can be significantly different from those on terrace atoms. An illustrative example is the faster dissociation of CO on Rh-(211) than Rh(111) by 9 orders of magnitude due to the step edges on Rh(211) that do not exist on Rh(111).[3] Although studies on single crystals have produced valuable information for the surface kinetics, single crystals are not representative of industrially relevant heterogeneous catalysts, such as small metal crystallites (1−10 nm) dispersed on high-surface-area oxides.

Recently, the so-called "materials gap" was bridged by two-dimensional arrays of nanoparticles and nanowires synthesized on oxide surfaces by electron-beam lithography[4] and size-reduction lithography.[5] The samples produced by these lithographic techniques possess metal/oxide interfaces that enhance reactivity[6] and resist poisoning during catalysis.[7] However, catalysts fabricated by lithography are inherently difficult to produce because of the lengthy fabrication process, costly equipment, inability to obtain high-density structures, and large size of the fabricated catalytic structures. To circumvent these limitations, alternative methods have been employed, such as ultrahigh vacuum metal vapor deposition on oxide surfaces,[8] which generally produces planar nanoparticle catalysts with irregular particles of a broad size distribution. Monolayer films of high density (∼10^{11} cm^{-2}) Pt nanoparticles of well-defined shapes and narrow size distributions have been produced on various oxide surfaces by Langmuir−Blodgett (LB) methods,[9] with the shape of the nanoparticles controlling the crystal facets exposed during synthesis.

Most commercial catalytic processes occur on nanoparticles under high pressures and elevated temperatures. Therefore, it is essential to perform in situ studies of the catalyst surface during reaction. Sum frequency generation (SFG) vibrational spectroscopy is a surface sensitive technique that has been successfully applied to various catalytic metal surfaces subjected to industrially relevant, high-pressure reaction conditions.[10] Since bulk Pt is centrosymmetric, its contribution to the SFG signal is usually negligible. Moreover, because isotropic gases do not generate SFG, the SFG signal can only be produced from the metal surface and the adsorbates on that surface, making SFG spectroscopy ideal for high-pressure conditions. Second-order nonlinear techniques have been primarily applied to flat substrates because of the ease of collection and analysis. However, most recently they have been used in surface studies of Pd nanoparticles vapor deposited on alumina[11] and solutions of submicrometer particles.[12]

* To whom correspondence should be addressed. Tel: 510-642-4053. Fax: 510-643-9668. E-mail: somorjai@socrates.berkeley.edu.

† Department of Chemistry, University of California, Berkeley, and Lawrence Berkeley National Laboratory.

‡ Department of Mechanical Engineering, University of California, Berkeley.

§ Current address: Harvard University, Department of Chemistry and Chemical Biology, Cambridge, MA 02138.

10.1021/jp062418a CCC: $33.50
Published on Web 07/27/2006

The primary objective of this investigation was to characterize CO adsorption and oxidation on cubic Pt nanoparticles deposited on single-crystal sapphire by SFG in total internal reflection (TIR) geometry. This technique is nondestructive and provides sensitivity and specificity for the nanoparticle surface and adsorbate. Another objective was to determine whether a coherent SFG intensity can be obtained from nanoparticles of less than 10 nm in size and if this signal would be sufficiently strong to monitor reaction kinetics. Since cubic Pt nanoparticles preferentially expose the (100) surface, the results can be directly compared with those of CO adsorption and oxidation on single-crystal Pt(100) surfaces.

2. Experimental Procedures

2.1. Synthesis and Assembly of Platinum Nanoparticles. Cubic Pt nanoparticles (face-to-face = 7.1 ± 0.6 nm and vertex-to-vertex = 9.4 ± 0.6 nm) were synthesized by a modified polyol process in the presence of poly(vinylpyrrolidone) (PVP) and Ag^+ ions.[9] An amount of 2.5 mL of ethylene glycol (EG) was refluxed for 5 min, and 0.5 mL of $AgNO_3$ solution (2×10^{-3} M, Ag/Pt = 1.1 mol %) was added to the boiling EG. Subsequently, EG solutions of PVP (93.8 μL, 0.375 M) and $H_2PtCl_6 \cdot 6H_2O$ (46.9 μL, 0.0625 M) were added to the mixture every 30 s over a 16-min period. The resulting solution was heated for an additional 5 min. The products consisting of ~80% cubes and ~10% tetrahedra (9.8 ± 0.7 nm) were purified by repetitive precipitation-centrifugation and finally dispersed in chloroform. Elemental analysis performed by inductively coupled plasma-atomic emission spectroscopy demonstrated that all Ag was incorporated into the Pt nanoparticles during synthesis.[13] The location and state of the Ag associated with the Pt nanoparticles is currently unknown. However, since detectable shifts were not observed by synchrotron-based X-ray diffraction, it is presumed that Ag is at the surface in the form of small clusters or isolated atoms.[14] Ethylene hydrogenation rates on Pt cubes supported on silica suggest that 1 at. % Ag does not have a detrimental effect on hydrogenation rates.[13] Previous studies have shown that pure Pt catalysts are ~50 times more active than a Pt−Ag catalyst with a much higher Pt/Ag molar ratio of 0.12,[15] where much of the surface is probably covered by Ag.

The Pt nanoparticles were assembled and deposited onto an equilateral single-crystal sapphire prism (Red Optronics, Mountainview, CA) by the LB technique. Colloidal Pt solutions were dispersed onto deionized water (18 MΩ·cm) subphase on a LB trough (NIMA Technology, type 611) at room temperature. The surface pressure was monitored with a Wilhelmy plate and adjusted to zero before spreading the particles. The resulting surface layer was compressed by moving a mobile barrier at a rate of 0.3 cm^2/min. At a surface pressure of 6 mN/m, the Pt monolayer at the water−air interface was carefully transferred onto the sapphire surface by the Langmuir−Schäffer horizontal liftoff method. Measurements obtained with an atomic force microscope (Park Scientific Instruments, Sunnyvale, CA) after scratching the surface with glass revealed a film thickness in the range of 10−11 nm. The films were observed in a JEOL 200CX transmission electron microscope to determine the shape and size distribution of the Pt nanoparticles.

2.2. Cell for in Situ Monitoring of Catalytic Reactions. A special cell was constructed for in situ SFG spectroscopy in TIR geometry under continuous gas flow conditions. An equilateral sapphire prism was held in compression against a rubber O-ring by tightening a Teflon block fitted to the prism apex to the body of the cell by two setscrews. The temperature at the prism surface was measured by a thermocouple placed directly on the sample. Heating was applied to the sides of the prism with two Kapton resistive elements (Omega Engineering, Inc., Stamford, CT). The temperature variation at the 20 × 20 mm^2 base area of the prism was insignificant. The reaction cell was connected to a 0.3175-cm-diameter stainless steel tubing gas manifold equipped with mass flow controllers (MFC, Porter Instrument Company) for precise delivery of the reactant gases, namely, CO (AirGas, CP grade), He (Praxair, UHP, 99.999%), and 20% O_2/He mixture (Praxair, UHP, 99.999%), all used in the as-received condition. A vacuum of <1 mTorr was maintained in the reaction cell by mechanical and sorption pumps.

The aforementioned flow reactor was slightly modified for gas chromatography (GC) measurements. The cell was reconfigured as a 0.2 L batch reactor with a recirculation pump that maintained a gas recirculation rate of >100 cm^3/min. The oxidation of CO was performed under excess oxygen conditions, i.e., 10 Torr CO and 100 Torr O_2. The accumulation of CO_2 with time was measured by a GC system (Hewlett-Packard 5880A) incorporated in the recirculation loop. A 20 ft long column (Carboxen 100, 80/100 packing density) was used to separate the CO, O_2, and CO_2 gases. Initial reaction rates were determined from plots of CO_2 accumulation vs time. The small total mass of Pt on the sapphire surface required kinetic data collection in batch mode. Depending on the reaction conditions, the time to accumulate a sufficient amount of CO_2 for GC detection ranged from several hours to a day.

2.3. SFG Vibrational Spectroscopy. SFG vibrational spectroscopy is ideal for studying the composition and conformational behavior at interfaces. SFG spectra were obtained with a Nd:YAG laser (Leopard, Continuum, Santa Clara, CA) by combining a tunable infrared (IR) beam with 532-nm radiation at the sample interface at corresponding incident angles of 60 and 65° with respect to the surface normal. The variation of the incident angle (±5°) produced a negligible effect on the measurements. A loosely focused area, IR energy of <10 μJ, and green energy of <50 μJ were used to minimize surface damage to the nanoparticles. For picosecond pulses (20 Hz) of duration equal to ~21 ps, the damage threshold of metals is low. Pulses of incident IR energy higher than 10 μJ or tightly focused spots resulted in discoloration and signal degradation over the course of the experiment.

A significant enhancement of the SFG signal can be obtained with Raman and IR active vibrational modes generated where centrosymmetry is broken.[16] Due to the complex nature of this system (e.g., dispersion and complex dielectric properties of the metal and nanoparticles) all data were collected at incident angles greater than the critical TIR angle by >15°. Different polarization experiments reflected the dielectric properties of the monolayer. However, ssp polarization combination signal yielded the highest signal-to-noise ratio. Thus, SFG results only for ssp polarization combination are presented here for brevity. A detailed description of the laser system used in this study can be found elsewhere.[17] Figure 1 shows a schematic of the optical setup for in situ SFG characterization of well-ordered nanoparticle monolayers.

Depending on the wavelength of the incident light, diffuse reflectance and scattering can be significant with rough surfaces. Rayleigh scattering and destructive interference for particle sizes less than the wavelength of incident light complicates the detection of the SFG signal. Additionally, the orientational freedom of the cubic nanoparticles and interaction with the substrate suggest that they might not be isotropic at the sapphire

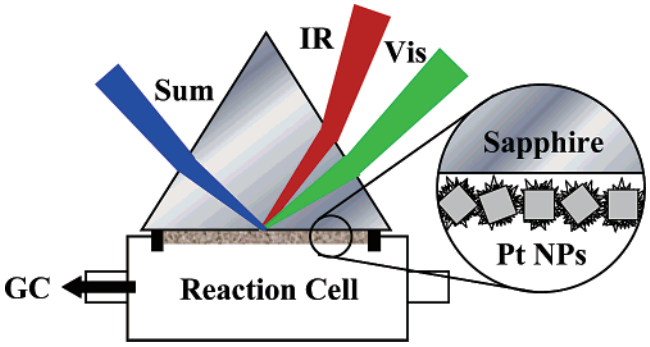

Figure 1. Schematic of in situ SFG reaction cell showing a monolayer consisting of PVP-capped Pt nanoparticles (NPs) deposited onto the single-crystal sapphire prism by a LB technique. The spectroscopy cell operates as a recirculating batch reactor. A gas chromatography (GC) system, incorporated in the recirculation loop, is used for periodic sampling of the gas-phase composition.

surface. These obstacles were overcome by using an internal reflection element (sapphire prism). Sapphire exhibits good transmission properties and good reflectivity from the interface of interest. Light scattering was not observed under the present experimental conditions. The TIR mode enhances the local fields and provides the additional benefit of signal intensification for centrosymmetric media. Since CO can adsorb on all exposed sides of the cubic nanoparticles, the inversion center would dramatically decrease the SFG intensity. It has been proposed that the exponential decay of the incident fields minimizes incoherent scattering and destructive interference.[18] Hyper-Rayleigh scattering is unlikely because the SFG signal is collected in the direction of momentum conservation.[19]

2.4. Quartz Crystal Microbalance. Quartz crystal microbalance (QCM) experiments were conducted under identical gas flow conditions using a QCM-D (Q-Sense) instrument. By monitoring the change in the resonance frequencies as a function of time, the mass change was related to the quantity of adsorbed gas. Samples of nanoparticles deposited on silica QCM disks, PVP spin-cast onto silica QCM disks, and Pt film vapor-deposited onto QCM disks were exposed to CO and the amount of irreversibly adsorbed CO was determined after purging with He until the baseline was stabilized.

3. Results and Discussion

3.1. Synthesis and Characterization of Nanoparticle Films. The assembly of 7.1-nm cubic nanoparticles by LB methods has been reported previously.[9] Deposition of a chloroform solution containing cubic Pt nanoparticles on the water surface increased surface tension due to the weakly bound PVP polymer. After lift-off at surface tension of 6 mN/m, the surface coverage was determined to be ~40%,[9] which corresponds to a nanoparticle number density of $\sim 7 \times 10^{11}$ cm^{-2}. The transmission electron microscopy (TEM) image of the nanoparticles deposited on a TEM grid, shown in Figure 2, reveals a uniform particle size and distribution. Atomic force microscopy (AFM) imaging of a scratched film demonstrated the formation of a smooth film with the expected thickness. The nanoparticle size and film thickness determined from TEM and AFM measurements were used to estimate the thickness of the capping polymer. The measured film thickness corresponds well with a 1−2 nm thick polymer coating on the 7.1-nm cubic nanoparticles.[20] The evaporation of chloroform did not affect the integrity of the monolayer. In fact, changes in the monolayer and nanoparticle shape could not be detected even after heating at 373 K in oxygen for 3 h. It has been reported that faceted Pt nanoparticles

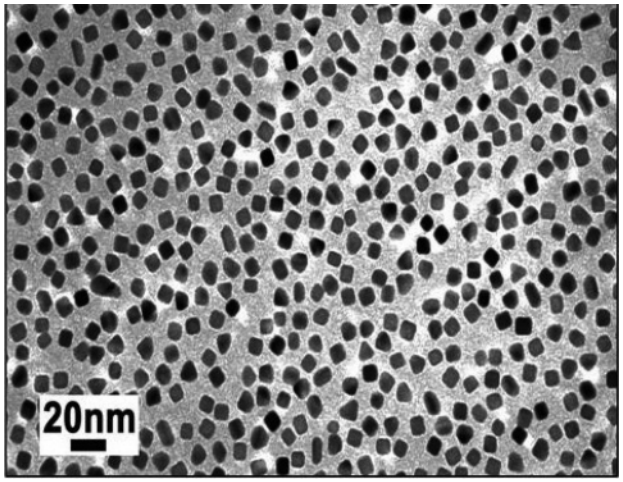

Figure 2. TEM image of a Langmuir−Schäffer monolayer consisting of PVP-capped Pt nanoparticles demonstrating that ~80% of the nanoparticles are cubes of 9.4-nm average size and ~10% tetrahedra of 9.8-nm average size.

of comparable size begin to melt and their corners round off upon heating at 623 K in a vacuum.[21]

3.2. CO Adsorption on Polymer-Covered and Oxidized Platinum Nanoparticles. The analysis of SFG vibrational spectra of the sapphire/nanoparticle interface obtained in ssp polarization combination was based on published data.[4] Control SFG experiments demonstrated that CO did not adsorb on a PVP film or a clean sapphire surface. The linearly bound (atop) CO peak on Pt is between 2060 and 2100 cm^{-1}, depending on the cleanliness of the metal substrate,[22] surface coverage,[23] and coordination number of the Pt atoms.[24] Atop CO molecules bound to step edges are usually attributed to peaks between 2060 and 2080 cm^{-1}.[25] The effect of the residual PVP coating on the monolayer surface was investigated by SFG spectroscopy. After purging the reaction cell with He gas to remove oxygen and water vapor, SFG spectra of the sapphire/nanoparticle system were obtained at room temperature in the presence of flowing CO. Figure 3 shows a comparison between SFG spectra of as-deposited and oxygen-pretreated (at 373 K for 3 h) monolayers exposed to CO at 295 K. The significant increase in atop CO peak intensity and shift toward higher frequencies in the spectrum of the pretreated monolayer is attributed to the water removal and the PVP decomposition. Thermal gravimetric analysis has shown that oxidation at 373 K removes hydrogen-bonded water and a small fraction of PVP. The remaining PVP can be completely decomposed by calcination in oxygen at temperatures above 623 K.[26] Although the decomposition kinetics is slow, Pt catalyzes the oxidative decomposition of PVP.[26] In the present study, the samples were heated at a temperature well below 473 K to avoid PVP densification as a result of cross-linking at this temperature.[27] According to hydrogen chemisorption measurements obtained at room temperature, approximately 50% of the surface of PVP-stabilized Pt colloids in 1-butanol is free of PVP and capable of adsorbing CO.[28]

A comparison of the spectra shown in Figure 3 indicates that the removal of water and/or PVP enhanced the CO peak intensity, most likely due to the increased availability of adsorption sites. The position of the absorption band also changed after oxidation, which may be due to the decreased interaction between adsorbed water and CO[29] or the increased dipole−dipole coupling between neighboring CO molecules.[30] Alternatively, CO adsorption onto a metal surface covered by oxygen atoms resulted in the blue-shift of the atop CO peak

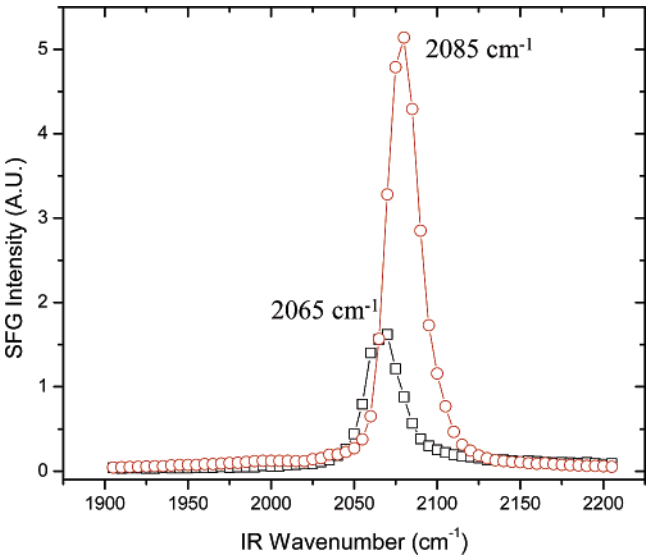

Figure 3. SFG spectra (ssp polarization) of a monolayer consisting of PVP-capped Pt nanoparticles exposed to CO at 295 K before (black squares) and after (red circles) oxidation in O_2 at 373 K for 3 h. Oxidation resulted in the removal of a significant fraction of the capping polymer, affecting the position and intensity of the CO peak.

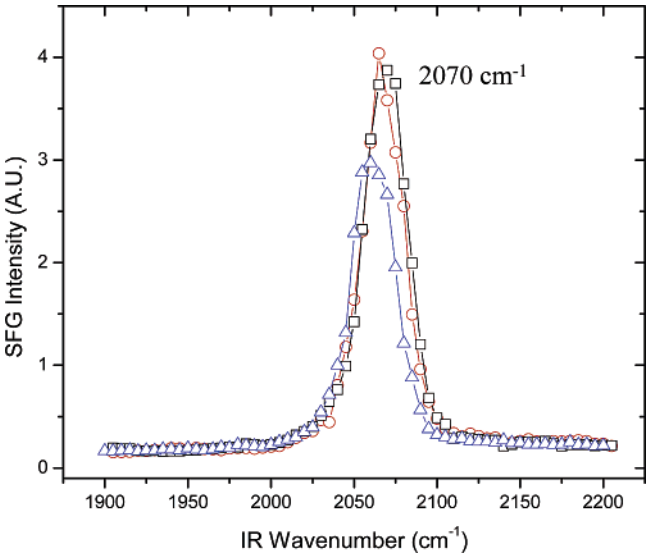

Figure 4. SFG spectra (ssp polarization) of a monolayer consisting of PVP-capped Pt nanoparticles previously treated in O_2 at 295 K obtained after successive exposure to (black squares) CO at 35 Torr, (red circles) He purging for 5 min, and (blue triangles) vacuum of <1 mTorr for 3 h. He purging caused a very small change in the CO peak. The red-shift of the CO frequency is attributed to water desorption and the enhancement of dipole−dipole coupling between neighboring CO molecules.

relative to CO adsorption onto a clean metal surface.[31] In addition, oxidation enhanced the nonresonant background and altered the dielectric properties of the particles, possibly modifying the local field intensities.[32] This pretreatment procedure (i.e., oxidation at 373 K for 3 h) was followed with every new sample before performing the kinetic experiments.

In another series of experiments performed at room temperature, SFG spectra of a monolayer pretreated in oxygen at room temperature were collected after each successive exposure to: (1) CO at 35 Torr, (2) He for 5 min, and (3) vacuum of <1 mTorr for 3 h. Figure 4 shows typical SFG spectra from these experiments. The strong peak illustrates the enhancement of CO chemisorption in the presence of the nanoparticles. The surfaces of face-centered cubic nanoparticles are terminated by atoms in the (100) orientation. CO binds strongly to the (100) facets, edges, and corner sites of the nanoparticle surfaces and less coordinated step and kink sites. The peak at 2070 cm^{-1} is assigned to atop bound CO, and is red-shifted significantly with respect to the CO peak for single-crystal Pt(100) (~2100 cm^{-1}). The 30-cm^{-1} shift is attributed to the PVP capping agent and the coadsorption of water from the ambient and/or airborne contaminants. At 35 Torr CO, all the available atop sites are occupied (maximum coverage conditions). The SFG spectrum of the monolayer exposed to CO at 35 Torr did not show any discernible changes even after a long exposure to CO (>24 h). The unchanged SFG spectrum after purging with He suggests that CO was strongly adsorbed onto the nanoparticles. Chemisorbed species are stable under a vacuum of <1 mTorr, yielding marginal changes in the SFG spectrum even after 3 h. The small decrease in the CO peak intensity after the exposure to a vacuum of <1 mTorr for 3 h is likely due to a small amount of desorbed CO or oxidation resulting from the prolonged duration of the experiment. Bridge-bound CO (~1850−1950 cm^{-1}) was not observed in any of these experiments. Since bridge-bonded CO is often undetected, the Raman transition moment of this species on Pt is likely low.[33]

In view of the sensitivity of the QCM technique to changes in the surface coverage of small samples, it was used under identical gas flow conditions to quantify the CO adsorption and estimate the availability of active Pt sites on the nanoparticle monolayer. First, a baseline was established by flowing He while collecting the QCM signal. Room-temperature experiments performed at atmospheric pressure with a LB-deposited nanoparticle film, 100 nm thick spin-cast PVP layer, and 10 nm thick vapor-deposited Pt film demonstrated mass changes with the introduction of CO into the reaction cell. Transient CO interaction ceased immediately upon subsequent purging with He, as indicated by the decrease in the apparent mass. Although the samples with the PVP and Pt films exhibited similar mass changes, a noticeable difference was observed after flushing the cell with He. While the PVP-coated sample recovered its original mass, the Pt film exhibited a mass gain of approximately 20−30 ng/cm^2. The LB nanoparticle sample demonstrated a different behavior. In addition to a larger amount of transiently adsorbed CO, a longer period was required for CO desorption to reach equilibrium. This could be related to a surface roughness difference or a tighter sievelike conformation of the PVP capping agent around the nanoparticles. The CO that was not removed by He purging was strongly adsorbed onto the nanoparticle and vapor-deposited Pt films. A comparison of the residual CO content with the intensity of the SFG signal demonstrated the sensitivity of SFG spectroscopy to submonolayer coverage by CO. In addition, the identical SFG spectrum after purging with He confirmed the negligible effects of transiently bound CO on the SFG signal. QCM measurements of the nanoparticle monolayer exposed to CO at room temperature (obtained after flushing with He) showed a mass gain of ~30 ng/cm^2 (normalized to the total QCM disk area). For an assumed Pt:CO ratio of 1:1, this mass gain represents a number density of active Pt sites equal to $\sim 7 \times 10^{14}$ cm^{-2}. By assumption of five exposed faces for each nanoparticle, this density of active Pt sites corresponds to a CO coverage of ~0.35, implying that ~65% of the nanoparticle surface area was contaminated by adsorbed water and organics.

3.3. In Situ Oxidation of CO on Clean Surfaces of Platinum Nanoparticles. After heating the samples at 373 K in oxygen for 3 h to remove the water and contaminants, CO

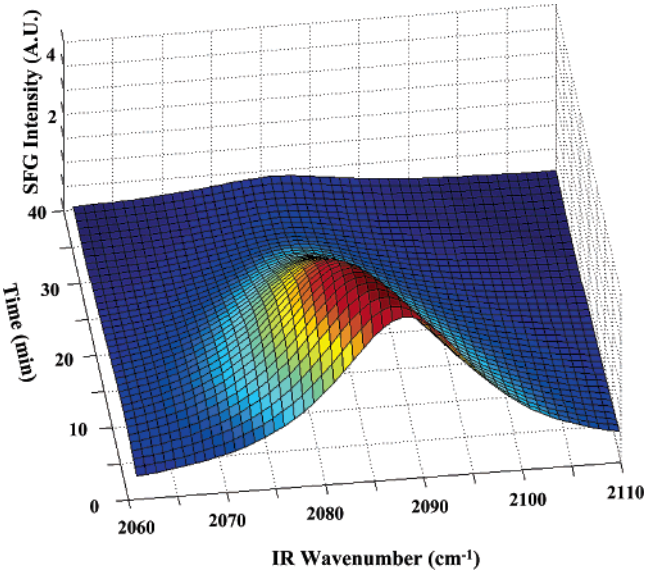

Figure 5. Lorentzian curve fits to SFG spectra (ssp polarization) of a CO-saturated monolayer consisting of PVP-capped Pt nanoparticles exposed to O_2 at 338 K obtained in intervals of 20 s. A red-shift of the CO atop peak emerges as the reaction proceeds and CO is removed from the surface by oxidation to CO_2. The monolayer was first heated in oxygen for 3 h and then purged with He at 373 K before exposure to CO.

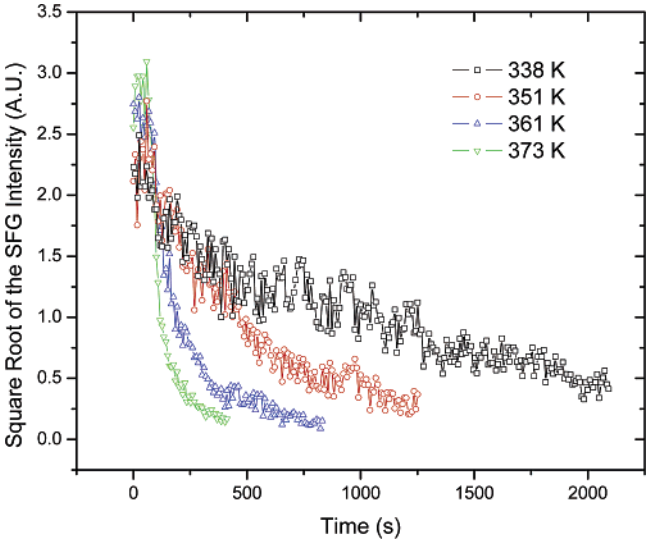

Figure 6. Square root of the atop CO peak intensity in the SFG spectrum (ssp polarization) of a monolayer consisting of PVP-capped Pt nanoparticles vs time under conditions of flowing O_2 at (black squares) 338 K, (red circles) 351 K, (blue triangles) 361 K, and (green upside-down triangles) 373 K.

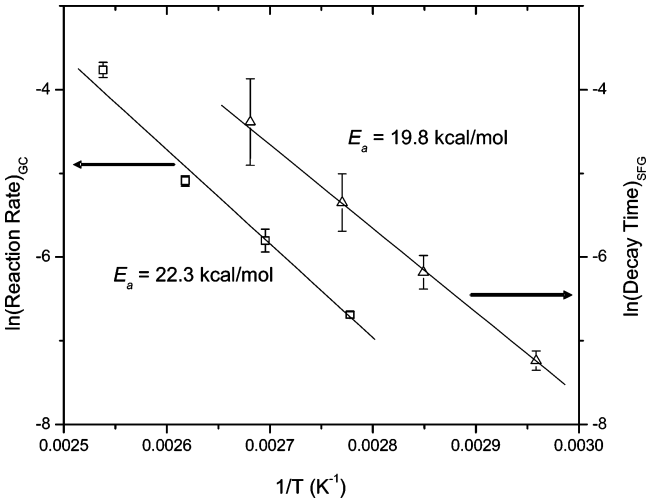

Figure 7. Arrhenius plots of CO oxidation measured by the first-order exponential decay of the SFG intensity of the atop CO peak (blue triangles) and the accumulation of CO_2 in the gas phase determined from GC measurements (black squares). The apparent activation energies calculated by the two independent methods are in good agreement with each other and with reported values for single-crystal Pt(100).

was introduced into the reaction cell for 5 min. It was observed that CO adsorption was spontaneous. Subsequently, the cell was purged with He for 10 min to remove any residual gas-phase CO, and SFG spectra were obtained in 1-min intervals while the cell was flushed with O_2/He (10/90 vol %) at 338 K, acquiring 50 shots for each data point at increments of 5 cm^{-1} in the range of 2060−2110 cm^{-1}. Figure 5 shows Lorentzian curve fits to SFG spectra collected every 20 s in ssp polarization during oxidation. Similar to previous SFG results, the CO peak exhibited a red-shift during oxidation.[34] The CO peak decayed continuously with the increase of time and disappeared after 40 min. Since He did not affect the CO peak intensity over the same time period, it is concluded that the removal of CO from the surface was mainly due to oxidation.

After an identical oxygen pretreatment for 3 h, CO was introduced at 373 K for 5 min and the system was flushed with He for >10 min prior to initiating oxidation by flowing O_2/He (10/90 vol %) at different temperatures. Each data set was repeated three times. The signal-to-noise ratio was sufficiently high to obtain kinetic measurements within a narrow frequency range that included the maximum of the atop CO peak. The intensity was monitored in the 2080−2085-cm^{-1} range at ~8-s intervals, collecting 50 shots for each data point at temperatures in the range of 338−373 K. Since the red-shift spanned a small frequency range during the course of the experiment (e.g., see Figure 5), this narrow range was used to reduce the acquisition time. Figure 6 shows representative exponential decay curves of the square root of the atop CO peak intensity at different temperatures. The square root of the CO peak intensity is used because the SFG intensity is proportional to the square of the number density of contributing groups.[16] The complex effect of dipole coupling on the IR absorption cross section[35] and the dependence of the SFG intensity on the possible reorientation of adsorbed CO during oxidation[16] were ignored by assuming a linear dependence of the square root of the SFG intensity on CO coverage. Although a linear relationship between SFG intensity and CO coverage has also been observed by other investigators,[36] a complex dependence of the SFG signal intensity on the CO coverage has been reported for high CO coverage of Ni(111) surfaces.[37]

The curves shown in Figure 6 were fit to a first-order exponential decay constant and an Arrhenius plot was constructed from the temperature dependence of the first-order decay constant. The rate dependence on temperature was also measured by standard chromatographic methods. Reaction rates were measured as a function of temperature by applying a linear fit to the CO_2 signal of the integrated thermal conductivity detector. Figure 7 shows a comparison of reaction kinetics determined from SFG and GC data in excess oxygen (100 Torr O_2 and 10 Torr CO). The similar activation energies determined by the two methods support the former assertion that oxidation was the primary reaction pathway. The calculated activation energy E_a of ~19.8 kcal/mol by SFG and 22.3 kcal/mol by GC is slightly higher than 13 kcal/mol measured for Pt(100) under stoichiometric conditions.[38] Measurements of catalytic activity

as a function of temperature for different $CO:O_2$ tend to give different apparent activation energies due to changes in the adsorption thermodynamics and surface coverage by individual adsorbates.[38] The activation energy for desorption on the Pt(100) surface is equal to ~30 kcal/mol.[39] This provides further support to the view that the decrease in the CO peak intensity was due to surface oxidation. The good agreement between the two techniques validates the linear relationship of the atop CO peak intensity and the CO surface coverage.

The origins of the nonlinear susceptibility and the enhancement resulting from local field interactions are complex. Monitoring the decay of an adsorbed species provides results in agreement with quantitative measurements. Recent SFG studies indicate that solution synthesized nanoparticle sizes important to catalysis do not produce SFG in external reflection when molecules adsorb on both the top and the bottom sides of the particles.[40] Despite the complex centrosymmetric system and unclear origin of the SFG signal in TIR, the results illustrate the potential of SFG spectroscopy. Additionally, monitoring reaction rates by standard chromatographic techniques is not practical in some cases of two-dimensional nanoparticle arrays due to the very small amount of the reaction products. This limitation can be circumvented by the TIR-SFG technique. Although the disappearance of a surface-bound species is an indirect measure of a reaction rate, the present technique enables in situ monitoring with the added benefit of simple and fast data collection. For example, a kinetic curve for CO oxidation on a small Pt surface area can be obtained with the present technique in less than 20 min. This is significantly faster than the several hours or even days needed to monitor initial reaction rates by GC at similar temperatures on small Pt surface areas.

4. Conclusions

SFG vibrational spectroscopy was successfully applied to a model nanoparticle system in total internal reflection geometry to enhance the signal intensity. A high-pressure reactor system that enables in situ SFG characterization and reaction studies of nanoparticle monolayers was used in this study. Coherent SFG measurements were obtained without the need for bulk gas absorption correction or complex dielectric considerations. CO is a model adsorbate because of its inherently strong SFG signal that makes it amenable to facile detection. CO adsorption was studied on as-synthesized LB films and films treated in oxygen to remove the residual PVP. The CO adsorption increased significantly upon the removal of PVP due to the increased availability of active sites. This increase in the CO coverage resulted in the red-shift of the atop CO peak due to the enhancement of dipole−dipole coupling. The CO coverage of the pretreated nanoparticle monolayer was evaluated by quartz crystal microbalance measurements. The oxidation of a CO monolayer under flowing oxygen studied by in situ SFG revealed an additional red-shift of the CO peak with time and the simultaneous decay of the peak intensity. The apparent activation energy for CO oxidation was found to be in good agreement with previous results for single-crystal Pt(100) surfaces. GC experiments performed on the same Pt nanoparticle monolayers under the same experimental conditions confirmed the activation energy determined from the SFG measurements.

Acknowledgment. This research was funded by the Berkeley-ITRI Research Center (BIRC) under Fund No. 46101-23845-44-EKMAJ and the Director, Office of Energy Research, Office of Basic Energy Sciences, Materials Science Division, of the U.S. Department of Energy under Contract No. DE-AC02-05CH11231. One of the authors (R.M.R.) would like to acknowledge Ford Motor Company for financial support through a graduate fellowship administered by the Berkeley Catalysis Center.

References and Notes

(1) Somorjai, G. A. *Introduction to Surface Chemistry and Catalysis*; Wiley: New York; 1994.
(2) Boudart, M. *Adv. Catal*. **1969**, *20*, 153.
(3) Mavrikakis, M.; Bäumer, M.; Freund, H.-J.; Nørskov, J. K. *Catal. Lett.* **2002**, *81*, 153.
(4) Baldelli, S.; Eppler, A. S.; Anderson, E.; Shen, Y.-R.; Somorjai, G. A. *J. Chem. Phys*. **2000**, *113*, 5432.
(5) Contreras, A. M.; Grunes, J.; Yan, X.-M.; Liddle, A.; Somorjai, G. A. *Catal. Lett.* **2005**, *100*, 115.
(6) Somorjai, G. A.; Rioux, R. M. *Catal. Today* **2005**, *100*, 201.
(7) Grunes, J.; Zhu, J.; Yang, M.; Somorjai, G. A. *Catal. Lett.* **2003**, *86*, 157.
(8) Henry, C. R. *Surf. Sci. Rep*. **1998**, *31*, 231.
(9) Song, H.; Kim, F.; Connor, S.; Somorjai, G. A.; Yang, P. *J. Phys. Chem. B* **2005**, *109*, 188.
(10) Su, X.; Cremer, P. S.; Shen, Y. R.; Somorjai, G. A. *J. Am. Chem. Soc*. **1997**, *119*, 3994.
(11) Dellwig, T.; Rupprechter, G.; Unterhalt, H.; Freund, H.-J. *Phys. Rev. Lett.* **2000**, *85*, 776.
(12) Roke, S.; Roeterdink, W. G.; Wijnhoven, J. E. G. J.; Petukhov, A. V.; Kleyn, A. W.; Bonn, M. *Phys. Rev. Lett.* **2003**, *91*, 258302.
(13) Rioux, R. M.; Song, H.; Grass, M.; Habas, S.; Niesz, K.; Hoefelmeyer, J. D.; Yang, P.; Somorjai, G. A. *Top. Catal*. **2006**, in press.
(14) Habas, S.; Yang, P., unpublished work.
(15) Campostrini, R.; Caturan, G.; Baraka, R. M. *J. Mol. Catal.* **1993**, *78*, 169.
(16) Shen, Y. R. *The Principles of Nonlinear Optics*; Wiley: New York; 1984.
(17) Kweskin, S. J.; Komvopoulos, K.; Somorjai, G. A. *Langmuir* **2005**, *21*, 3647.
(18) Yeganeh, M. S.; Dougal, S. M.; Silbernagel, B. G. *Langmuir* **2006,** *22*, 637.
(19) Bohren, C. F.; Huffman, D. R. *Absorption and Scattering of Light by Small Particles*; Wiley: New York; 1983.
(20) Su, M.; Bai, C.; Wang, C. *Solid State Commun.* **1998**, *106*, 643.
(21) Yu, R.; Song, H.; Zhang, X.-F.; Yang, P. *J. Phys. Chem. B* **2005**, *109*, 6940.
(22) Ferri, D.; Bürgi, T.; Baiker, A. *J. Phys. Chem. B* **2001**, *105*, 3187.
(23) Eischens, R. P.; Francis, S. A.; Pliskin, W. A. *J. Phys. Chem*. **1956**, *60*, 194.
(24) Brandt, R. K.; Sorbello, R. S.; Greenler, R. G. *Surf. Sci.* **1992**, *271*, 605.
(25) Mukerji, R. J.; Bolina, A. S.; Brown, W. A. *Surf. Sci.* **2003**, *527*, 198.
(26) Rioux, R. M.; Toops, T. J.; Grass, M.; Niesz, K.; Yang, P.; Somorjai, G. A., to be submitted 2006.
(27) Yoshida, M.; Prasad, P. N. *Appl. Opt.* **1996**, *35*, 1500.
(28) de Caro, D.; Köhler, J.; Busser, W.; Bradley, J. *Macromol. Symp.* **2000**, *156*, 53.
(29) Rupprechter, G.; Dellwig, T.; Unterhalt, H.; Freund, H.-J. *J. Phys. Chem. B* **2001**, *105*, 3797.
(30) Persson, B. N. J.; Ryberg, R. *Phys. Rev. B* **1981**, *24*, 6954.
(31) Cant, N. W.; Donaldson, R. A. *J. Catal.* **1981**, *71*, 320.
(32) Westerberg, S.; Wang, C.; Chou, K.; Somorjai, G. A. *J. Phys. Chem. B* **2004**, *108*, 6374.
(33) Su, X.; Cremer, P. S.; Shen, Y. R.; Somorjai, G. A. *Phys. Rev. Lett.* **1996**, *77*, 3858.
(34) McCrea, K. R.; Parker, J. S.; Somorjai, G. A. *J. Phys. Chem. B* **2002**, *106*, 10854.
(35) Hoffmann, M. F. *Surf. Sci. Rep*. **1983**, *3*, 107.
(36) Härle, H.; Metka, U.; Volpp, H.-R.; Wolfrum, J. *Phys. Chem. Chem. Phys.* **1999**, *1*, 5059.
(37) Bandara, A.; Katano, S.; Kubota, J.; Onda, K.; Wada, A.; Domen, K.; Hirose, C. *Chem. Phys. Lett.* **1998**, *290*, 261.
(38) Berlowitz, P. J.; Peden, C. H. F.; Goodman, D. W. *J. Phys. Chem*. **1988**, *92*, 5213.
(39) McCabe, R. W.; Schmidt, L. D. *Surf. Sci.* **1977**, *66*, 101.
(40) Pang, S. F.; Kurosawa, Y.; Kondo, T.; Kawai, T. *Chem. Lett*. **2005**, *34*, 544.